Mitotic Chromosome Structure: Reproducibility of Folding and Symmetry between Sister Chromatids

Yuri G. Strukov[‡] and A. S. Belmont[†‡*]
[†]Department of Cell and Developmental Biology, and [‡]Biophysics Program, University of Illinois, Urbana-Champaign, Illinois

ABSTRACT Mitotic chromosome structure and pathways of mitotic condensation remain unknown. The limited amount of structural data on mitotic chromosome structure makes it impossible to distinguish between several mutually conflicting models. Here we used a Chinese hamster ovary cell line with three different *lac* operator-tagged vector insertions distributed over an ~1 μm chromosome arm region to determine positioning reproducibility, long-range correlation in large-scale chromatin folding, and sister chromatid symmetry in minimally perturbed, metaphase chromosomes. The three-dimensional positions of these *lac* operator-tagged spots, stained with *lac* repressor, were measured in isolated metaphase chromosomes relative to the central chromatid axes labeled with antibodies to topoisomerase II. Longitudinal, but not axial, positioning of spots was reproducible but showed intrinsic variability, up to ~300 nm, between sister chromatids. Spot positions on the same chromatid were uncorrelated, and no correlation or symmetry between the positions of corresponding spots on sister chromatids was detectable, showing the absence of highly ordered, long-range chromatin folding over tens of mega-basepairs. Our observations are in agreement with the absence of any regular, reproducible helical, last level of chromosome folding, but remain consistent with any hierarchical folding model in which irregularity in folding exists at one or multiple levels.

INTRODUCTION

The large-scale structure of mitotic chromosomes and the mechanisms underlying chromosome condensation remain elusive after more than four decades of experimental efforts. Chromosomal proteins and protein complexes with enzymatic activities necessary for condensation and maintenance of chromosome structure have been identified and studied in vitro; however, their actual in vivo functions are still unclear (1–3). Similarly, from a structural point of view, the number of distinct levels of chromatin compaction involved in the transition between interphase and mitotic chromosomes remains unknown. The apparent irregularity of chromosome folding is one of the major challenges in deciphering chromosome structure. This irregularity makes it difficult to define, isolate, or study individual structural elements of chromosomes. Other factors complicating the analysis of chromosome structure include the extremely high compaction of chromatin within mitotic chromosomes and the sensitivity of native chromatin morphology to even slight changes in the ionic strength of the environment.

A number of different models of mitotic chromosomes can be roughly divided into two, apparently mutually conflicting groups. Radial-loop type models are based largely on observations of mitotic chromosomes after extensive extraction of chromosomal proteins. This treatment is aimed at relaxation of tightly compacted chromatin to reveal its substructure. According to radial-loop models, loops of 30 nm chromatin fibers are attached to a nonhistone protein ''scaffold'' through DNA-protein interactions (4,5). The estimated size of these loops measured by different methods and in different species varies between 20 and 150 kbp. Later modifications of the radial-loop model suggested that the ''scaffold'' of each chromatid is helically coiled rather than corresponding to a simple linear arrangement of the loop bases (6,7).

Instead, hierarchical coiling models are derived from experiments designed to avoid, or at least minimize, perturbation of the native chromosome morphology. Hierarchical coiling models assume that the DNA molecule is either regularly or irregularly coiled into a hierarchy of distinct folding motifs, with each higher-level folding unit formed by coiling of a lower-level folding motif (8–11). It may be that both types of mitotic chromosome models are valid for reflecting different aspects of mitotic chromosome structure.

However, neither model group explicitly addresses the more basic question of the DNA folding reproducibility within mitotic chromosomes. Here ''folding reproducibility'' refers to both comparisons of identical chromosomes isolated from different cells and comparisons of folding between sister chromatids of the same chromosome. The question of folding reproducibility is critical for ultimately understanding the underlying mechanisms of chromosome condensation.

Chromosome-specific banding patterns along the longitudinal mitotic chromosome axis observed after certain treatments are one of the most prominent, reproducible features of mitotic chromosome structure (12–14). These banding patterns demonstrate reproducibility in the folding of DNA sequences with respect to position along the chromosome axis on a DNA sequence scale of several mega-basepairs (Mbp). How reproducible folding is on a smaller scale, and how reproducible positioning of specific DNA sequences is transverse to the chromosome axis remain unknown.

Submitted August 11, 2008, and accepted for publication October 21, 2008.

*Correspondence: asbel@uiuc.edu

Editor: Alberto Diaspro.

0006-3495/09/02/1617/12 $2.00

doi: 10.1016/j.bpj.2008.10.051

Besides the observed reproducible banding patterns, other experimental results have suggested the existence of additional levels of order within mitotic chromosomes. These may be related to chromosome banding patterns, or perhaps even the cause of these banding patterns, or they may be independent of these banding patterns.

A helical structure of topoisomerase IIα axial staining, proposed to be part of a chromosome scaffold, was observed after partial extraction of histone H1 using a polyanion-containing buffer (6). However, only ~1% of chromosomes showed regular helical coiling of scaffolds, with sister chromatids related by mirror symmetry, and most chromosomes instead formed misshapen ''halos''. More recently it was suggested that this apparent helical coiling may reflect over-condensation of chromosomes in a small fraction of cells induced by prolonged exposure to mitotic inhibitors (15). It therefore remains unclear whether symmetry between sister chromatids is present in mitotic chromosomes with minimally perturbed morphology.

Reproducible positioning of specific DNA sequences relative to the longitudinal axes of chromatids was suggested based on fluorescence in situ hybridization (FISH) experiments. The same peripheral or axial positioning in both prometaphase and metaphase chromosomes for several specific probes was described (16). This led to a model in which the transition between prophase and metaphase chromosomes involved progressive shortening of the chromosome axis and further condensation without significant reorganization of sequences transverse to the chromosome axis. However, the actual differences in sequence distribution observed in that study were not dramatically different from those expected for a random distribution. Moreover, interpretation of these results was further complicated by possible systematic experimental errors. The FISH procedure used in that study included harsh conditions of fixation and DNA denaturation, and clearly led to chromosome flattening, suggesting a significant perturbation of chromosome morphology that might have led to significant large-scale rearrangement of DNA sequences (16).

In contrast, highly reproducible targeting of specific, gene-amplified DNA sequences to the metaphase chromatid axes was previously observed in mammalian chromosomes, and no obvious regularity or symmetry was seen in the positions of these same spots in prophase or telophase chromosomes (17). These results suggested a more pronounced structural transition between prophase and metaphase. More recently, light and electron microscopy of artificial chromosome regions containing *lac* operator repeats suggested the existence of a 200–300 nm folding subunit in metaphase chromosomes (18). Of interest, immunogold staining of these regions suggested a distinct lack of reproducibility in positioning transverse to the chromosome axis.

These varied results prompted a reexamination of the question of reproducibility of DNA sequence folding within mitotic chromosomes using the *lac* operator/*lac* repressor system, which permits labeling of specific regions in minimally perturbed, formaldehyde-fixed chromosomes (19). Here we report results suggesting the absence of reproducibility in lateral positions of specific sequences in mitotic chromosomes as well as a lack of strict symmetry in DNA folding between sister chromatids. We show that even though condensation of sister chromatids is precisely spatially and temporally coordinated, they follow independent condensation pathways. These results are discussed in terms of models and mechanisms of mitotic condensation.

MATERIALS AND METHODS

Cell line and cell culture

MC8_I Chinese hamster ovary (CHO) cells, a derivative of the DG44 cell line (20), were grown in F-12 (HAM) medium (Gibco BRL, Boston, MA) lacking thymidine and hypoxanthine and supplemented with 10% dialyzed fetal bovine serum (FBS; HyClone, Salt Lake City, UT) and 0.25 μM methotrexate (MTX; Molecular Probes, Eugene, OR). The C6 cell line (21) was created after transfection with a 15 kbp supercoiled plasmid pSV2DHFR-8·32 carrying a 256mer *lac* operator direct repeat (19). MC8_I CHO cells were isolated after gene amplification of the C6 cells.

Isolation and immunofluorescence staining of mitotic chromosomes

Isolation of mitotic chromosomes was carried out according to a previously published protocol with modifications (22). CHO cells in a 75 cm^2 flask, grown to confluency, were incubated for 2.5 h with media supplemented with 600 ng/mL nocodazole, which was then replaced with fresh media without nocadazole. After 15 min of incubation, mitotic cells were detached from the surface by gentle shaking of the flask, collected into a 50 mL conical tube, and sedimented at 500 *g* for 10 min at +4°C. After hypotonic treatment with 75 mM KCl at 37°C for 10 min, the mitotic cells were centrifuged at 500 *g* and vortexed in a small volume of buffer PA (15 mM Tris-HCl, 0.2 mM spermine, 0.5 mM spermidine, 2 mM EDTA, 0.5 mM EGTA, 80 mM KCl, 20 mM NaCl, pH 7.2 at +4°C) containing 0.1% digitonin. Isolated chromosomes were deposited on 12 mm round glass coverslips (#1.5; Fisher Scientific, Pittsburgh, PA) by centrifugation at 3000 *g* for 10 min at +4°C and then fixed with 1.6% formaldehyde (Polyscience, Pittsburgh, PA) in PBS* for 10 min at room temperature (PBS* is PBS with 5 mM $MgCl_2$ and 0.1 mM EDTA; PBS (1 liter): 8.00 g NaCl, 2.16 g Na_2HPO_4*($7H_2O$), 0.20 g KCl, 0.20 g K_2HPO_4 in deionized water, pH 7.4). Staining of fixed chromosomes with *lac* repressor was performed as described elsewhere (23). Staining for topoisomerase IIα was done for 24–48 h at +4°C in PBS supplemented with 0.5% BSA (Sigma, St. Louis, MO) using primary rabbit topoisomerase IIα antibody at 1:30 dilution (24). Texas Red-labeled secondary antibodies were used for detection of *lac* operator sequences, and fluorescein isothiocyanate (FITC)-labeled secondary antibodies were used for topoisomerase IIα. DNA was stained with either 0.2 μM/mL 4′,6-diamidino-2-phenylindole (DAPI) or 0.5 μM/mL propidium iodide in PBS*.

Microscopy and image processing

Three-dimensional (3D) optical sections were collected with an Olympus IMT-2 inverted fluorescence microscope with an Olympus 60×/NA 1.4 objective and a cooled Photometrics CCD camera. Voxel size was 74 nm in the *x* and *y* directions, and 100 nm along the optical axis. All images of chromosomes were corrected for the CCD dark current, variations in the microscope illumination field, and variations in the gain between individual pixels, as well as for mercury lamp brightness variations, and then

deconvolved as described previously (25) with calculated point spread function. Images were analyzed with Newvision (26) and ImageJ (http://rsb.info.nih.gov/ij/). All quantitative analysis of images was done with MATLAB 6 (The MathWorks, Natick, MA). The scripts used in this work are available upon request.

Chromatic aberration measurements and control of accuracy of measurements of z-coordinates were done using fluorescent, multicolored micro beads (diameter: 90 and 560 nm; Molecular Probes, Portland, OR) deposited on glass coverslips. Suspensions of 90 and 560 nm diameter micro beads were diluted, mixed together, and deposited on round glass coverslips (Corning, Corning, NY) at a density of 200–500 beads of each size per square millimeter. The coverslips were air-dried and mounted with Prolong mounting medium (Molecular Probes).

RESULTS

Experimental system

In this work we used MC8_I cells derived in our laboratory from DG44 CHO cells. DG44 cells are CHO cells that contain a double deletion of the DHFR gene, induced by x-ray irradiation (20). DG44 cells were transfected with the pSV2DHFR-8.32 plasmid containing 256 copies of a 36 bp *lac* operator sequence (19). A stable cell line, C6, containing 10–20 copies of the pSV2DHFR-8.32 transgene inserted at a single chromosome site was selected (21). This C6 cell line was used for gene amplification, using methotrexate selection (19), to generate the MC8_I cell line.

One of the longer chromosomes within MC8_I cells contains a single chromatid region with three nearby transgene array sites, creating three closely spaced pairs of spots within the two sister chromatids of the metaphase chromosome (Fig. 1, *A–C*). Spots were located in the middle of the chromosome arm, away from both the centromere and telomere. A fourth spot is located on the opposite arm of the same chromosome. By light microscopy, the three *lac* operator-containing loci have the same appearance of diffraction limited spots of ~0.2 μm diameter. Variation between intensity levels in images of individual spots on the same chromosome was relatively small, which allowed us to treat individual spots as identical. These loci likely represent copies of the original C6 transgene insertion site, together with large stretches of flanking genomic CHO DNA generated by the gene amplification process. We found that MTX was necessary for maintenance of multiple inserts. If MTX was removed from the medium, cells with multiple spots were replaced by cells with a single pair of spots after ~20 cell passages.

Chromosomes within intact mitotic cells are packed very densely, their orientation in three dimensions is random, and they are usually bent, which makes it difficult to follow chromatid axes. Therefore, for these experiments we used chromosomes isolated from mitotic cells and deposited by gentle centrifugation onto glass coverslips. Deposited on coverslips, the chromosomes appear straight and parallel to the glass surface (Fig. 1, *A* and *B*). The *lac* operator/*lac* repressor system was used for detection of transgene insertion sites (19), avoiding the harsh conditions used for the DNA denaturation required for FISH approaches and better preserving the 3D chromosome architecture.

By examining the 3D locations of the three pairs of *lac* operator-containing insertion sites in MC8_I cells, we were able to compare both the reproducibility of DNA folding in different metaphase chromosomes and the reproducibility in folding within the two sister chromatids from the same metaphase chromosome. Chromatid axes were detected by immunostaining against topoisomerase IIα (Fig. 1, *A–C*), which concentrates at the axial cores of isolated metaphase chromosomes (27–29). All chromosomes stained for *lac* op repeats showed six spots (three per sister chromatid) in this chromosome region, indicating that all inserts were detectable by antibody staining irrespective of their positions on mitotic chromosomes (Fig. 1, *A–C*). *Lac* operator spots could be located at the periphery of chromosomes as well as in internal regions between sister chromatids (Fig. 1 *B*).

Calibration and control of accuracy of measurements

Spot sizes corresponded to the diffraction limit of the fluorescence microscope. However, the spot centers can be determined much more precisely. The signal/noise ratio (>30) and photon counts (>1200) in images of chromosomes were high enough to guarantee that centroid calculations gave accurate estimates of the centers of the spots (30,31). Separate excitation filters were used for DNA (DAPI) and topoisomerase IIα signals, but both were detected with a single 537/30 nm emission filter. A 625/30 nm emission filter was used for detection of *lac* operator sequences immunostained with Texas-Red-labeled antibodies.

We found significant chromatic aberration shifts in the positions of multicolored beads imaged with two different emission filters (data not shown). Bead centroids were separated by $\Delta x = (20 \pm 7)$ nm, $\Delta y = (46 \pm 7)$ nm, $\Delta z = (345 \pm 15)$ nm, or 0.3, 0.6, and 3.5 pixels, respectively. Chromatic aberration was corrected by adjusting the calculated coordinates of the centroids of *lac* operator spots and chromatid axis positions by the calculated mean values in all images.

To estimate the accuracy of measurements of Z chromatic shift, suspensions of 90 and 560 nm diameter micro beads were air-dried on coverslips and mounted in an antifading agent. 3D stacks of optical sections were collected with 100 nm increments in the z-direction. Because of significant differences in the fluorescence intensity of the 90 and 560 nm beads, different exposures were used for different beads in the same field. The centroid of a fluorescent bead was defined as the center of intensity-weighted voxels. Images were thresholded such that levels below the threshold were set to zero and values above the threshold were unchanged. The measured centers of larger and smaller beads sitting close to each other on the coverslip surface were separated by 220 ± 30 nm (mean ± SD) in the axial direction,

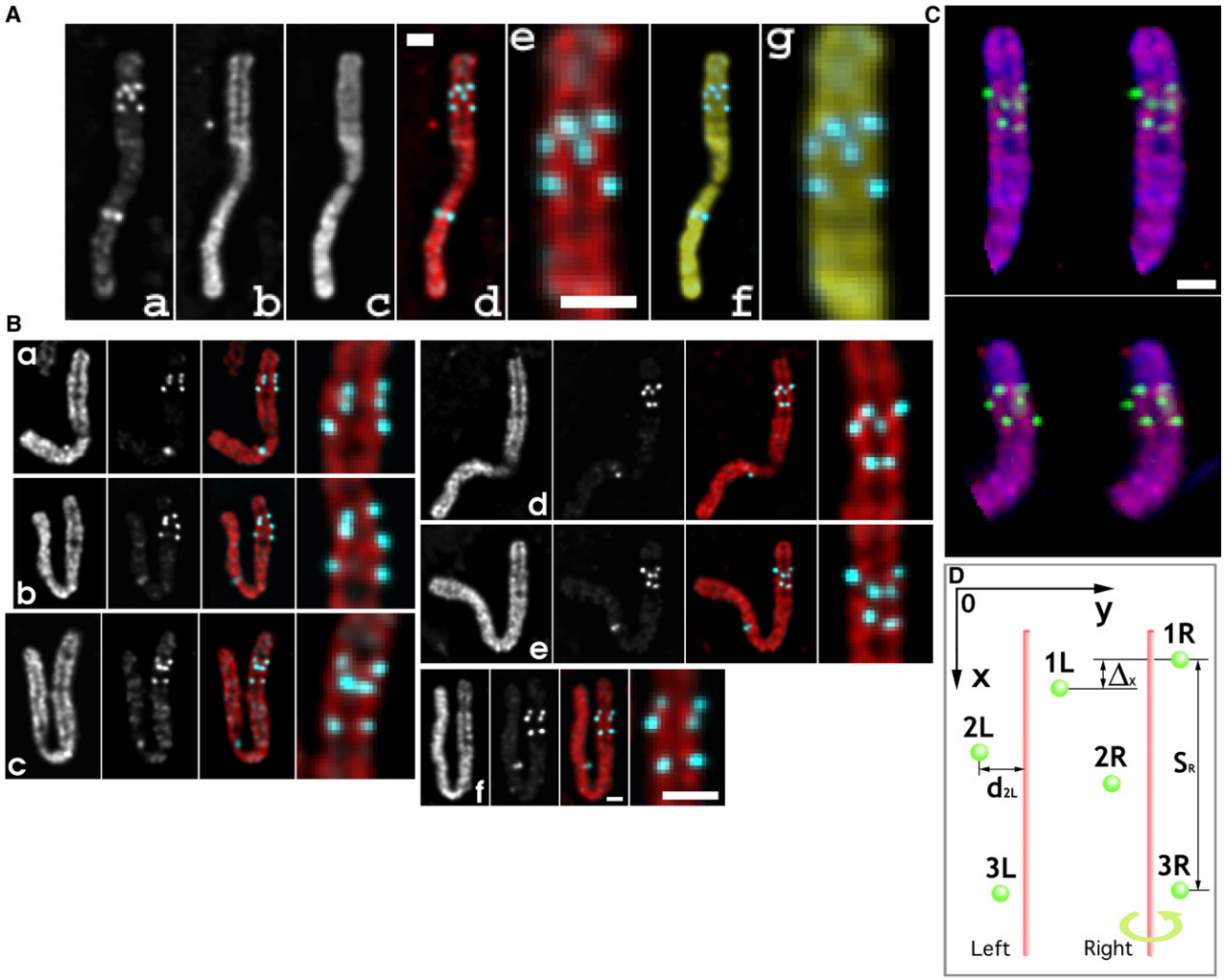

FIGURE 1 Visualization of longitudinal and axial positioning of closely spaced *lac* operator-containing vector inserts. Isolated mitotic chromosomes from the MC8_I clone show three nearby vector transgene sites (top chromosome arm), with a fourth transgene site on the opposite chromosome arm. *Lac* repressor and topoisomerase II staining labeled vector transgene sites and chromosome axes, respectively. (*A*): (*a*) *Lac* repressor staining of *lac* operator-containing vector insert sites; (*b*) anti-topoisomerase II antibody staining; (*c*) total DNA stained with DAPI; (*d*) merged *lac* repressor (*cyan*) and topoisomerase II (red) staining; (*e*) 3× enlargement from (*d*); (*f*) merged DAPI (*yellow*) and *lac* repressor signal (*cyan*); (*g*) 3× enlargement from *f*. (*B*): (*a–f*) Six examples of isolated metaphase chromosomes. Subpanels (*left* to *right*): topoisomerase II immunostaining, *lac* repressor staining, merged (topoisomerase II *red*, *lac* repressor *cyan*), merged, 3× enlargement. (*C*): Two stereo pairs of metaphase chromosomes reconstructed from optical sections. Total DNA stained with DAPI (*blue*), anti-topoisomerase II (*red*), and *lac* repressor staining (*green*). (*D*) 2D model of a fragment of a chromosome with *lac* op inserts: *lac* op spots, green; sister chromatid axes, red. Bars: 1 μm.

close to the predicted 230 nm separation. Variations in bead diameter, fluorescent labeling throughout the bead interior, and deformation of coverslip surfaces could also contribute to the observed discrepancy between predicted and measured values. Shifts due to chromatic aberration and relative *z* coordinates of the beads were highly reproducible as demonstrated by measurements done on the same samples several days later.

The 3D positions of centers of *lac* operator-tagged spots within mitotic chromosomes were also calculated by measuring centroids of spots after thresholding. The shape of the microscope point spread function with poor resolution along the *z* axis made it difficult to extract 3D coordinates of the topoisomerase-labeled chromosome axes; therefore, 2D projections of the axes were used with the assumption that the axes of isolated chromosomes were parallel to the surface of coverslips. To find the axes of mitotic chromosomes, deconvolved optical sections with topoisomerase IIα immunostaining signal were projected and two maxima of intensity in each row of pixels perpendicular to chromatid axes (one per chromatid) were detected. These maxima of topoisomerase IIα immunostaining corresponded to the central regions of daughter chromatids. The curves corresponding to the central regions of chromatids were calculated by fitting a low-degree polynomial using the measured chromatid centers. The segments of the central curves, with positions and lengths limited by the coordinates of the spots

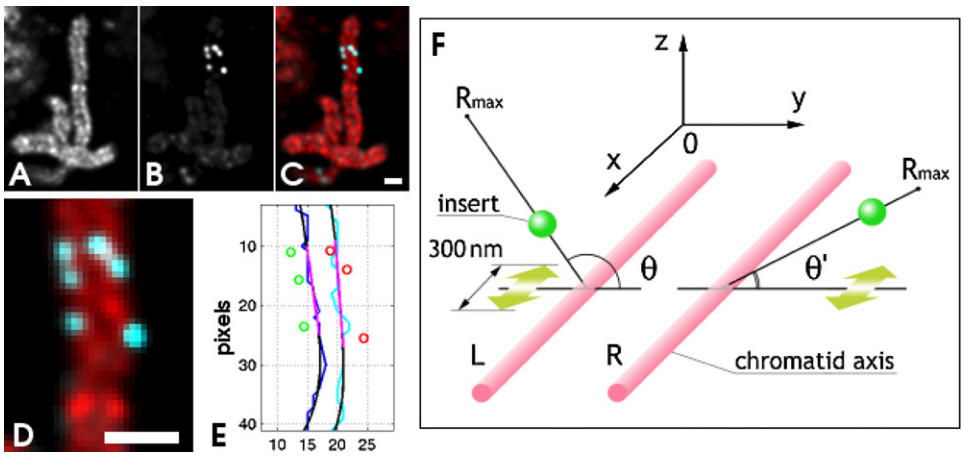

FIGURE 2 Quantitative analysis of an imaged CHO metaphase chromosome with *lac* operator inserts. (*A*) Anti-topo II immunostaining. (*B*) *Lac* op immunostaining. (*C*) Superimposition of *A* and *B*. (*D*) 3× enlarged region from *C*. (*E*) Extraction of geometrical parameters from *D*: (*green* and *red*) centers of extracted 3D coordinates of *lac* op spots of left and right chromatids, respectively; (*blue* and *cyan*) traces of centers of topo II signal for left and right chromatid axes, respectively; (*black* and *pink*) 4th degree polynomial and linear fits of axes traces, respectively. (*F*) Model of metaphase chromosome used for Monte Carlo simulation. The distance between a spot and the chromatid axis was distributed uniformly between 0 and R_{max}; angles θ and θ' were distributed uniformly between 0 and 2π. Spot positions in sister chromatids were assigned independently, modeling the absence of any correlation of spot positioning in sister chromatids. Bars: 1 μm.

1 and 3 (Fig. 1 *D*), were approximated by linear segments using a line fit (Fig. 2, *A–E*).

Longitudinal positions of inserts on daughter chromatids vary within an ~250 nm range

The high correlation between sister chromatid lengths and perfect registration of chromosomal bands could result from physical connections established by cohesin complexes between sister chromatids during mitotic condensation (32). Cohesins do not disassociate from chromosomal arms completely until the metaphase-anaphase transition, although release of cohesins from chromosomal arms starts in prophase and precedes release from centromeric regions (33). Even though chromosomal bands, or large, multicopy vector inserts (18), appeared to have the same longitudinal positions in sister chromatids, a comparison of the longitudinal positions of the small inserts in the MC8_I cell line revealed variation in the spot positions between sister chromatids.

The original images of 97 chromosomes with three pairs of spots were rotated so that the chromosomes were parallel to the *x* axis, with the origin set close to the telomere of the chromosome arm with the multiple spots (Fig. 1 *D*). For easier reference, the pairs of spots were numbered 1 (closest to the telomere) through 3 (closest to the centromere). Pairs 1 and 3 were separated longitudinally by 1.0 ± 0.2 μm (mean ± SD; min 0.5, max 1.4), representing ~70 Mbp of the CHO genome (23). The length of the chromosomal arm containing the inserts is 6.3 ± 1.1 μm (mean ± SD; min 1.0, max 9.9). Between sister chromatids there remains significant variation in the longitudinal distance, *S*, separating spots 1R and 3R, or 1L and 3L (Fig. 1 *D*), and *S* values for sister chromatids are weakly correlated ($r^2 = 0.33$; Fig. 3 *A*). Distance *S*, as expected, is correlated with the length of the chromosome arm (Fig. 3 *B*), although this correlation is not strong ($r^2 = 0.48$; Fig. 3 *B*).

We next calculated relative differences between the longitudinal coordinates for a single pair of spots on sister chromatids of the same chromosome (Δ_x for left and right chromatids; Fig. 1 *D*). The difference in longitudinal positions of ''sister'' spots varies approximately between −300 nm and 300 nm (Fig. 3 *C*). Averaging over all chromosomes, longitudinal separation between ''sister'' spots is 0 ± 120 nm (mean ± SD, min −280 nm, max 320 nm). The average value of absolute separations for all three pairs together is 90 ± 70 nm (mean ± SD, min 0, max 320).

If the longitudinal distance, *S*, between spots 1 and 3 of the same sister is normalized to one for each chromatid for all chromosomes, then the distances between spots 1 and 2 (e.g., 1R to 2R) are on average over all chromatids 0.36 (min 0.12, max 0.59, SD 0.09). The histogram distribution of normalized distances between spots 1 and 2 (Fig. 3 *D*) supports the observation that longitudinal positions of specific sequences in mitotic chromosomes are reproduced with little variation. There is no correlation, however, between the longitudinal distances between spots 1 and 2 of the sister chromatids ($r^2 = 0.02$). This is because the distance between spots 1 and 2 is comparable in length to the random deviation from average position, and the random deviations of individual spots are not correlated.

These numbers could be explained by random positioning of spots within perfectly registered, bandlike ~300 nm thick fibers in sister chromatids. Of interest, 200–300 nm is roughly the width of chromatin fibers previously observed in mitotic chromosomes (18). Even though DAPI staining produced banding patterns that are similar and registered in sister chromatids, longitudinal positions of the same specific, relatively short sequences of sister chromatids are not strictly fixed and correlated. It is interesting to note that patterns formed by the anti-topo II antibody staining are roughly symmetrical between sister chromatids in terms of large-scale longitudinal variation in labeling intensity and appear similar for different chromosomes, and probably have the same origin as the DAPI banding pattern (Fig. 1 *B*).

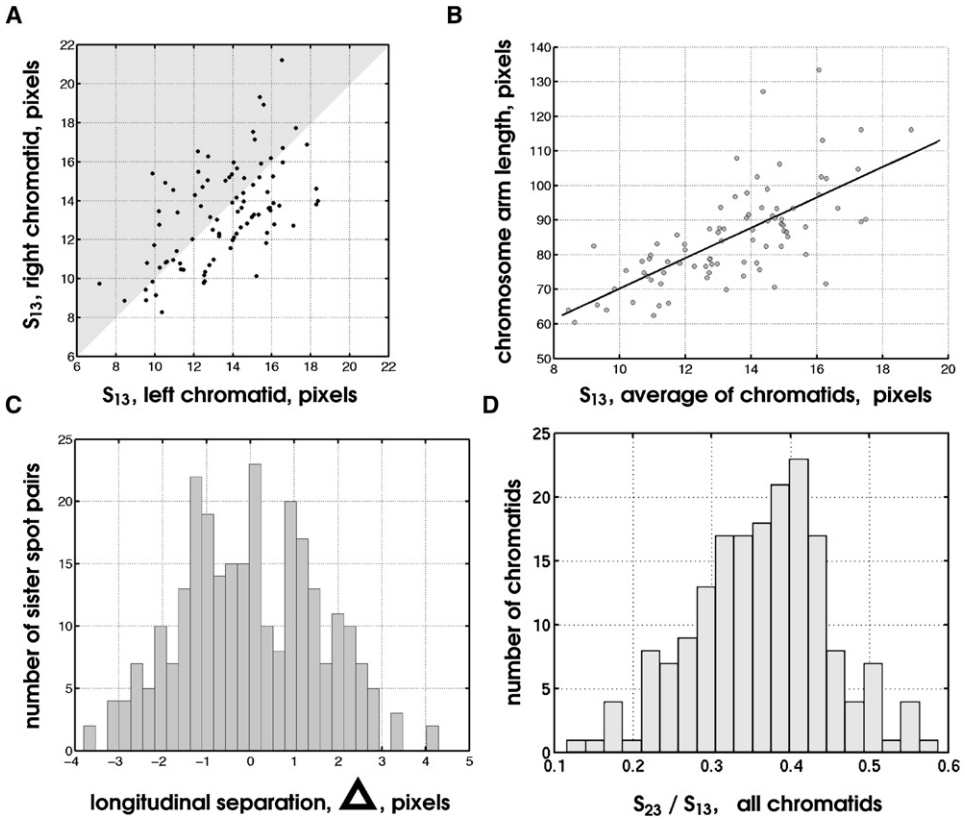

FIGURE 3 Longitudinal spot positions are reproducible but show significant variability. (*A*) Distances between spots 1 and 3 (Fig. 1 *D*) vary significantly between sister chromatids. Scatter plot where each spot corresponds to measured distances on the left and right chromatids for a particular metaphase chromosome. (*B*) Correlation between chromatid arm length versus longitudinal separation of spots 1 and 3, with plotted values representing average of measurements on sister chromatids. (*C*) Longitudinal coordinates of individual spots vary within ~300 nm. Histogram of differences between longitudinal coordinates of "sister" spots, e.g., 1L and 1R. (*D*) Histogram of distribution of longitudinal distances between spots 1 and 2 normalized by distance between spots 1 and 3.

Vector inserts do not occupy fixed positions with respect to chromatid axes

Relative to the longitudinal positions, the axial coordinates of the inserts showed a greater variability. Distances from the spot centers to the chromatid axes were measured in 2D projections of 3D stacks of optical sections. Spots found on the left of the corresponding chromatid axis were given a positive axial coordinate, and spots on the right side were given a negative coordinate.

Spots did not have fixed and reproducible positions relative to the chromatid axes (Fig. 4, *A* and *B*, and Table 1). Histograms of lateral deviations from the axis for spot 1 of the left chromatid only (Fig. 4 *A*) and for all three pairs of both chromatids together (Fig. 4 *B*) show a slight bias away from the chromatid axis, with the average spot position 0.4–0.7 pixels (~30–50 nm) away from the calculated chromatid axis (Table 1). This observation is confirmed by plotting lateral deviation from the axis of the spots of the left chromatid versus deviations for the spot of the right chromatid (Fig. 4 *C*): the data points are more abundant in the area of the plot with positive abscissa and negative ordinate. In other words, this means that the *lac* op spots, and possibly the rest of the DAPI-labeled DNA, are more likely to be found outside the metaphase axes than between them. Lateral positions of the sister spots are not correlated with each other ($r^2 = 0.08$).

One possible explanation for the observed randomness is that the imaged chromosomes represent a range of condensation levels or stages, and that more fixed locations would be observed within a given subset of chromosomes with similar degree of condensation. To test whether this is the case, the deviation of the projected spot position from the chromosome axis was plotted as a function of chromosome arm length for the top pair of spots of each chromosome (Fig. 4 *D*). The distribution of points in Fig. 4 *D* demonstrates that the lateral position of a spot and the length of the chromosomal arm are not correlated in 2D projections. Chromosomal arms of the same length show different spot patterns: the spots can occupy any axial position within a chromatid, both internal and external.

This real data set was compared with Monte Carlo computer-generated data (Fig. 2 *F*) obtained using the following model: Longitudinal positions of the simulated spots were determined by the average of measured positions of spots from the real chromosomes. Spots were allowed to deviate randomly with a uniform distribution within a 300 nm range as suggested by the observed data. Specifically, the distribution of the relative difference between the longitudinal positions of sister spots has a shape close to a triangle centered at zero relative difference (Fig. 3, *C* and *D*). This triangle shape is consistent with the convolution of two independent rectangular probability distributions, which would be the consequence of a uniform distribution for each spot and no correlation for longitudinal position between sister chromatids.

The longitudinal distance between spots 1 and 3 (e.g., 1R to 3R as in Fig. 1 *D*) varies significantly due to variations in

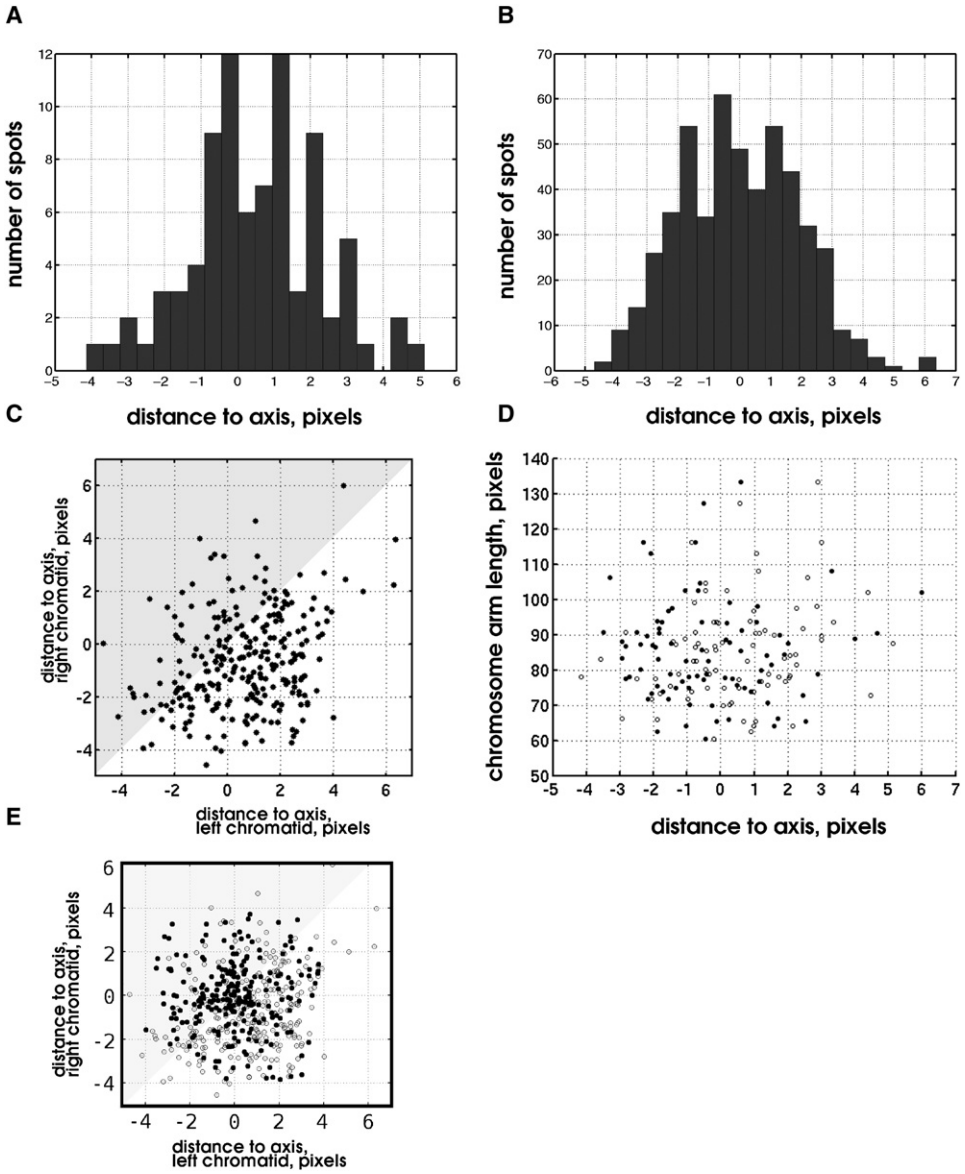

FIGURE 4 Lateral positions of individual spots relative to chromatid axis are nonreproducible, uncorrelated between sister chromatids, and independent of the degree of chromosome condensation. (*A*) Distance histogram for spot 1L to chromatid axis. Positive distances correspond to spots located on the left (*exterior*) of the chromatid axis, and negative distances correspond to spots on the right (*interior*) of the axis. (*B*) Histogram of axial positions for all spots. (*C*) Scatter plot showing comparison of lateral spot positions for sister chromatids: left spot (x axis) versus right spot (y axis). (*D*) Axial position versus length of chromosomal arm for the top pair of *lac* op spots of all chromosomes; (*gray circles*) right chromatids; (*solid circles*) left chromatids. (*E*) Scatter plots from 2D projections of actual (*open circles*) and simulated (*black circles*) chromosome measurements demonstrate comparable distributions for axial positions of *lac* operator spots. Mean values, SDs, and absence of correlation between sister chromatids were similar for experimental and simulated distributions.

the length of chromosomal arms. A random stretching factor was used for simulated chromosomes to make distributions of their geometrical features close to the observed data. Distances from a spot to a chromatid axis were assumed to be uniformly distributed between 0 and R_{max}, where R_{max} was taken from experimental data, and axial angles θ and θ' were assumed to be uniformly distributed between 0 and 2π. The model also assumed that the radial and axial positions of given spots were not influenced by the other spots on the chromosome (Fig. 2 *F*). Several hundred chromosomes were generated using Monte Carlo simulation according to this model. Chromosomes generated with the computer according to the described ''random folding'' model produced distributions of the measured geometrical features, such as absolute and relative longitudinal and lateral positions of ''sister'' spots or spots of the same chromatid similar to the imaged chromosomes in terms of mean values and SDs. For imaged and simulated chromosomes, the average distances from spots to the chromatid axis were 1.3 ± 1.0 and 1.6 ± 1.1 pixels, respectively (mean ± SD). The similarity of distributions of lateral positions of *lac* op spots in 2D projections between imaged and simulated chromosomes is demonstrated in Fig. 4 *E*. This finding supports the idea

TABLE 1 Mean distances (SD) from spots to the corresponding axes of chromatids in pixels in 2D projections (absolute distances to the axes and axial coordinates for each spot are shown)

	Left chromatid		Right chromatid	
Spots	Absolute distance, pixels	Distance, pixels	Absolute distance, pixels	Distance, pixels
First pair	1.46 (1.13)	0.54 (1.76)	1.57 (1.07)	−0.40 (1.86)
Second pair	1.71 (1.21)	0.74 (1.96)	1.61 (1.10)	−0.72 (1.81)
Third pair	1.63 (1.01)	0.59 (1.83)	1.53 (1.00)	−0.72 (1.68)

that chromosome condensation occurs through irregular folding, at least at higher levels of organization.

Daughter chromatids compact independently

The results described above suggest two possibilities. First, they could be the consequence of an irreproducible and therefore irregular folding of chromatin, at least at the higher levels of folding within mitotic chromatids. Alternatively, folding of chromatin within individual daughter chromatids could be very reproducible; however, the two daughter chromatids may be rotated relative to each other within the metaphase chromosome, explaining the data presented above. In addition, it is possible that shortening of chromatids during mitotic condensation is accompanied by rotation of chromatids around their axes by certain angles. This, in turn, could lead to changes of the lateral positions of spots relative to the chromatid axes in 2D projections when the chromosomes are compared at different stages of condensation.

To test whether rotation was responsible for the significant variation in the lateral positions of the spots between sister chromatids, projections of the 3D spot locations or the three pairs of spots onto the *YZ* plane were examined. If condensation within chromatids followed the same pathways, then differences in relative positions of spots of different chromosomes would be due either to rotation of the chromatids during condensation relative to each other, or, alternatively, to the lack of a fixed orientation of one chromatid relative to the other. We found, however, that spot locations projected on the *YZ* plane are not related by rotation only. Some of them are in configurations that require not only rotation and stretching, but also mirror reflection to be superimposed with each other.

Specifically, using the fact that there were three pairs of spots on the same chromosome, we sought to determine whether it is possible to superimpose the spots of two daughter chromatids by rotating one of the chromatids. The spots of one chromatid were rotated around the chromatid axis by an angle and translated in three dimensions to provide the best superimposition of the spots of one daughter chromatid with the other (i.e., the root mean-square (RMS) distance was a minimum). The same procedure was applied to chromosomes after a mirror reflection of one of the chromatids (right) relative to a plane bisecting the two daughter chromatids.

The Optimization Toolbox of MATLAB was used to solve this optimization problem. The cost function, which was a sum of three squared distances between ''sister'' spots, was minimized over possible 2D or 3D translations of spots of one chromatid with respect to the other, and rotations of one of the chromatids around its axis, with the other chromatid being fixed. Optimization was done for both 2D projections (Fig. 5, *A* and *B*) and 3D data (Fig. 5, *C* and *D*) for real and Monte Carlo simulated data. For the 2D case, the RMS distance between sister spots in 2D projections was minimized through translation of the dots of the right chromatid relative to the left chromatid in *X* and *Y*. Calculations were repeated for 2D projections after the spots of the right chromatid were replaced with their mirror reflection with respect to the chromatid axis. Comparisons of distributions of the minimized RMS for all chromosomes have not revealed any preference for the original chromosomes or for chromosomes in which the right chromatid was substituted with its mirror reflection. Some sister chromatids show a configuration of sister spots that is close to translational symmetry, some chromatids look more mirror-symmetrical, and in a fraction of chromosomes the sister spots cannot be superimposed at all (Fig. 5, *A* and *B*). Similar calculations were done with the 3D data. RMS minimization between spots of sister chromatids in 3D was done through 3D translation and rotation of spots of the right chromatid around an axis parallel to its axis. The distribution of minimized distances was found to be similar for both original and mirror-reflected chromatids.

No correlation between the inferred symmetry of chromatids and compaction, estimated by the length of chromosomal arms, was observed. For example, for 2D projections, the average lengths of chromosomal arms for all chromatids showing translational symmetry was 6.5 ± 0.9 μm (mean $\pm$ SD) and 6.1 ± 1.2 μm (mean $\pm$ SD) for mirror symmetry-related chromatids. The minimized (through translation and rotation around chromatid axes) mean-square distances were similar for the original chromosomes and for chromosomes where one of the chromatids was mirror-reflected.

The results obtained from computer-generated data (using the model summarized in Fig. 2 *F*) were similar to the results from the real data, suggesting that there is little correlation between positions of spots on daughter chromatids due to significant variations in lateral positions, and that chromatids condense independently of each other.

DISCUSSION

Our work was motivated by longstanding questions concerning mitotic chromosome condensation. Do specific sequences occupy fixed positions in mitotic chromosomes? Is there any correlation in the relative positions of sequences separated by distances of up to several tens of Mbp? And finally, is there any symmetry or reproducibility in the large-scale chromatin folding of daughter chromatids?

Our first goal was to examine the reproducibility of chromatin folding within minimally perturbed isolated metaphase chromosomes. Although we cannot rule out some structural perturbation caused by the chromosome isolation conditions, our procedure exploited everything we have learned about buffer conditions and isolation protocols to minimize structural changes. Certainly our procedures are significantly improved relative to those used in all previous experiments using FISH procedures. Using cell lines containing several nearby vector inserts of small size, we show that the axial

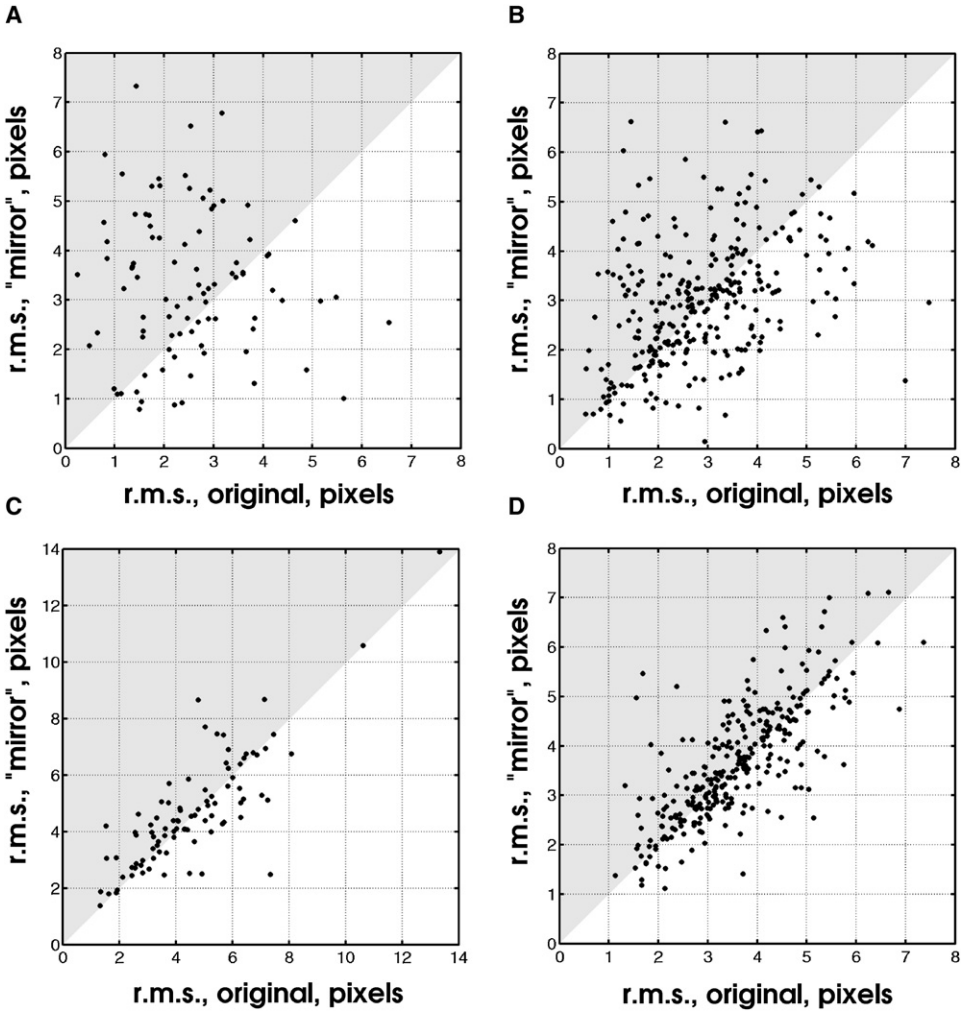

FIGURE 5 Similar distributions of spot positions relative to chromatid axes for real and computer-generated data. Minimal RMS deviations in pixels for spots of sister chromatids were found through an optimization procedure between original chromosomes (*abscissa*) and chromosomes in which a mirror reflection of the right chromatid was performed (*ordinate*). The left chromatid was fixed. For the right chromatid, 2D translation and rotation of the projection was allowed for the 2D case (*A* and *B*), and 3D translation and rotation around the chromatid axis was allowed for the 3D case (*C* and *D*). (*A*) 2D projections, real data. (*B*) 2D projections, simulated data. (*C*) 3D real data. (*D*) 3D simulated data.

positions of spots vary among different chromosomes and therefore are not reproducible. Our second goal was to study correlation between the large-scale structures of sister chromatids in a metaphase chromosome. We found that the large-scale folding patterns of daughter chromatids, as judged by distributions of vector inserts, are independent of each other and do not show translational or mirror symmetry. Similarly, we found no correlation between lateral positions of spots of the same chromatid. In the cell line used in this work, neighboring spots are separated by ~30–40 Mbp of DNA, which corresponds to several mitotic bands. These results argue against any long-range correlation in chromatin folding over tens of Mbp distances, as might be predicted in a regular, helical organization.

Our results are inconsistent with simple, highly ordered helical models or more general hierarchical folding models for mitotic chromosome structure, which invoke a high degree of folding reproducibility across multiple levels of chromatin folding. However, they remain consistent with hierarchical chromosome folding models, in which large-scale mitotic chromatin is formed through irregular successive compaction of lower-level chromatin fibers.

Improvement of the detection technique

Here we describe an experimental approach to study the large-scale structure of mitotic chromosomes by investigating the distribution of specific sequences in isolated chromosomes with preserved large-scale structure. It is challenging to study the structure of mitotic chromosomes experimentally, for several reasons: the tight compaction of the chromatin, the susceptibility of the large-scale chromatin structure to changes in ionic conditions, and the physical limits of resolution of fluorescence microscopy.

Extraction of chromosomes, a popular technique, is used to partially or completely decondense tightly packed mitotic chromatin in an attempt to decompose the chromosome into the structural elements that comprise the original chromosome, and hence enable visualization of those elements. The question remains, however, as to whether ''halos'' of extracted chromosomes are adequate simplifications of intact chromosomes and may be used to infer the original large-scale structure of chromatin before extraction. Experiments with extracted chromosomes have led to the radial-loop models of mitotic chromosomes. However, there is no evidence

from experiments on intact chromosomes that the loop-like structures are present. A hierarchically folded chromatin fiber that is held compact by certain chromosomal proteins, such as topoisomerase II and condensins, may turn, after extraction of histones and other soluble proteins, into an artificial set of loops attached to a resistant to extraction core or ''scaffold''. These covalent or noncovalent complexes of DNA and ''scaffold'' proteins withstand extraction. The size of the loops may reflect the frequency of the sites at which DNA interacts with the ''scaffold'' proteins. It was hypothesized that the so-called SAR (Scaffold Associated Region) sequences may serve as such ''anchor'' DNA sequences responsible for interaction with ''scaffold'' proteins. Indeed, it has been shown that SAR sequences remain bound to interphase nuclear matrices after high salt extraction, and specifically and cooperatively interact with topoisomerase II.

Large-scale structures are highly susceptible to changes in the ionic strength of the environment. This is why we made measurements on isolated, formaldehyde-fixed metaphase chromosomes with preserved morphology, at least at the level of light microscopy. The chromosomes were not subjected to any treatment that causes large-scale rearrangements of chromatin, including dehydration, unlike the FISH-based detection techniques used in previous studies (16,22), which included partial or complete extraction, fixation with methanol: acetic acid, and drying of chromosomes. It has been proposed that there could exist two distinct processes of mitotic condensation. The first stage is characterized by condensation of chromatin into prophase chromosomes. After the chromosomes split into two chromatids, the second stage is distinguished by extra coiling of chromatids (regular or irregular) (34). We cannot exclude the possibility that prolonged incubation of mitotic cells with colchicine induces further condensation of chromatids. This may have led to the mirror or other types of symmetry between sister chromatids observed in earlier studies (6,7,16), but did not occur in our experiments, which used shorter mitotic arrest protocols.

Finally, resolution of conventional fluorescent light microscopy is limited by ~200 nm perpendicular to the optical axis, which makes it difficult to observe the fine structural elements of chromosomes. Electron microscopy has better resolution; however, it is more difficult and tedious to collect data and preserve unperturbed large-scale structure in samples for electron microscopy. Optical rather than physical serial sections may be used in fluorescence microscopy. Our methodology allowed us to measure accurately, with subpixel accuracy, the 2D positions of fluorescently labeled vector inserts. Resolution along the optical axis was lower due to the fundamental limitations of light microscopy.

No strict order and reproducibility within mitotic chromosomes

We found that individual spots do not occupy fixed reproducible lateral positions on chromatids. Lateral positions of individual spots may change within the entire width of a chromatid width, which is ~400–500 nm, while longitudinal positions vary within only an ~300 nm, bandlike region. One explanation for this observation is that condensation of chromatids is not reproducible and does not follow one established scenario for each mitosis, and the large-scale chromatin structure is irregular. Alternatively, chromatids could rotate around their axes relative to each other during condensation by a random angle; then 2D projections of individual specific DNA sequences would not have fixed lateral positions even when each chromatid follows the same condensation pathway. However, measurements of the 3D positions of spots exclude the possibility that folding of chromatids is reproducible, as sister chromatids in different examples show neither mirror nor translational symmetry.

An alternative explanation for the lack of positioning reproducibility is that the observed variability among chromosomes is the result of their being caught at different stages of condensation. Even though nocodazole treatment blocks the cell cycle at prometaphase, the degree of chromosome compaction might depend on the block duration. We therefore tested whether axial spot positioning might be a function of chromosome length, and therefore the degree of chromosome condensation, but no correlation was observed.

Our observations of chromosome geometry fit into several different models of mitotic chromosomes, all involving irregularity of folding at one or multiple levels. Specifically, one possibility is that the 200–300 nm large-scale chromatin fiber observed in earlier studies (8–10) is folded irregularly and nonreproducibly to form the final 400–600 nm chromatid. Within the 200–300 nm chromatid, specific sequences could occupy positions that are reproducible from mitosis to mitosis. The opposite possibility is that the 200–300 nm fiber is coiled regularly in a larger mitotic chromatid, but that lower levels of chromatin folding within this 200–300 nm fiber are irregularly folded. This second possibility would explain the longitudinal variability in spot positioning and at least some of the considerable axial variation. A third possibility is that irregularity of folding occurs at multiple levels of chromosome organization.

Sequence-specific, reproducible banding patterns in isolated and mitotic chromosomes imply a certain degree of order as well as spatial correlation between daughter chromatids. Specific sequences are always found within the same bands/regions of mitotic chromosomes.

It is possible that reproducibility is limited to the lower levels of chromatin compaction, and the higher levels observed during mitosis are more independent. We claim that at least for a fraction of chromatin, reproducibility of chromosome condensation is limited only to the longitudinal and not the lateral positioning of specific sequences, which is consistent with the phenomenon of chromosomal banding. Previous results suggest, however, that a subset of DNA sequences may be reproducibly targeted to specific regions of mitotic chromosomes (17).

Daughter chromatids are spatially not correlated with each other

It has been known for a long time that linear dimensions of sister chromatids in mitosis are highly correlated, with the length, width, and banding patterns of chromatids of the same chromosome being the same at different stages of mitotic condensation. Previous studies have reported ''mirror'' symmetry between daughter chromatids (6,16). This implies precise coordination between chromatids due either to close bonds between chromatids—mediated, for instance, by sister chromatid cohesion until their separation in anaphase—or to a regular and reproducible condensation process. Here we argue that daughter chromatids do not possess symmetry and compact independently of each other. In previous work, we examined the chromosomal folding of band-sized chromosome regions formed by multicopy vector insertions carrying *lac* operator repeats (18). Anti-*lac* repressor immunogold staining was combined with electron microscopy to visualize these chromosome band-like structures by the vector insertions. These results showed that the minimal-size, *lac* operator-containing chromosome band was ~200–300 nm wide, and that these band-like structures showed sharp borders within the same chromatid, and formed structures of similar shape, size, and width within sister chromatids, but that ''sister'' bands might not register exactly between sister chromatids. These results are consistent with the general idea that sequences are distributed throughout a 200–300 nm band structure formed by the folding of a fiber of the same width as the band. The degree of misregistration of *lac* operator-containing bands in sister chromatids requires further analysis, but could explain at least part of the longitudinal variation in spot position we observed in this work. However, it seems that again an additional level of irreproducibility of folding must be invoked to explain the observed variation in axial positioning of sequences.

Similarly, topoisomerase II distribution demonstrates distinctive substructure at the core regions of chromosome arms consisting of foci of different sizes connected in a linear manner along the chromosome length. Occasionally, a helical structure is suggested. However, sister chromatids show similar misregistration in the density of anti-topoisomerase II staining similar to that described above for the bands of *lac* operator-containing chromatin (Fig. 1). The apparent lack of symmetry in axial distributions of topoisomerase II also argues against strict spatial correlation between sister chromatids. The variable longitudinal distribution of topoisomerase II, as well as many other chromosomal proteins, may arise from the same underlying mechanism as the formation of chromosome banding patterns, which are related to DNA sequence content or protein distributions (e.g., cohesin-mediated linking of homologous sequences).

If mitotic condensation of chromatids is spatially uncorrelated, then the interactions between daughter chromatids are not fixed and may break and reestablish frequently during mitotic condensation, or they are not necessarily sequence specific. Lack of symmetry between daughter chromatids in 2D projections may be due to both nonreproducible irregular folding of chromatids and/or rotational freedom of chromatids. It is interesting that in human tissue culture cells, residual cohesins have been localized between late metaphase chromatid axes (33). This suggests that at least for a small fraction of DNA sequences, either their positions are correlated between the sisters or cohesins link nonhomologous DNA fragments.

We found that more *lac* op spots are found outside both sister chromatid axes, as marked by anti-topo II antibody staining, than between the axes. This interesting observation may reflect the fact that DNA in sister chromatids is not distributed axially uniformly around the axes at this stage of mitosis, probably due to residual cohesion links, with more DNA found at the periphery of metaphase chromosomes. It remains to be seen whether cohesins, which are always found between axes of sister chromatids, have a preference for certain regions of chromatin or DNA and influence distribution of DNA in mitotic chromosomes.

Future directions

Previous attempts to study large-scale mitotic chromosomes were hindered by the absence of methods for labeling of specific DNA sequences in morphologically intact chromosomes. A *lac* repressor/*lac* operator detection system allows labeling of chromosomes with preserved structure as well as observation of tagged chromatin regions in live cells in vivo. Further improvements in spatial resolution (and in the axial direction specifically) of fluorescent microscopes would allow investigators to measure the positions of spots and chromatid axes with higher accuracy to build 3D models of chromosomes at different stages of condensation. A closer look at positioning of different types of DNA sequences (such as active versus silent DNA, or early-replicating versus late-replicating) with respect to chromosomal cores could be also informative. Our results do not exclude the possibility that the lack of reproduced lateral positions of specific sequences in mitotic chromosomes comes from variations in angular positions (e.g., angles Θ and Θ' in Fig. 2 *F*) of sequences with fixed radial deviations away from chromatid axes. Observation of mitotic condensation in live cells, following temporal rearrangement of specific DNA sequences relative to each other during mitosis, could help to establish intermediate condensation steps separating interphase versus mitotic chromosome structure. Finally, more needs to be known about the nature of the forces driving mitotic chromatin condensation, and the roles of specific chromosomal proteins and their modifications in establishing these forces.

We thank Dan Sullivan for providing generous advice and the antibody against topoisomerase IIα.

This work was supported by grant No. R01 GM42516 from the National Institute of General Medical Sciences, National Institutes of Health (A.S.B). The content is solely the responsibility of the authors and does not necessarily represent the official views of the National Institute of General Medical Sciences or the National Institutes of Health.

REFERENCES

1. Maeshima, K. and M. Eltsov. 2007. Packaging the genome: the structure of mitotic chromosomes. *J. Biochem.* 143:145–153.
2. Gassmann, R., P. Vagnarelli, D. Hudson, W. C. Earnshaw. 2004. Mitotic chromosome formation and the condensin paradox. *Exp. Cell Res.* 296:35–42.
3. Swedlow, J. R., and T. Hirano. 2003. The making of the mitotic chromosome: modern insights into classical questions. *Mol. Cell.* 11:557–569.
4. Marsden, M. P., and U. K. Laemmli. 1979. Metaphase chromosome structure: evidence for a radial loop model. *Cell.* 17:849–858.
5. Paulson, J. R., and U. K. Laemmli. 1977. The structure of histone-depleted metaphase chromosomes. *Cell.* 12:817–828.
6. Boy de la Tour, E, and U. K. Laemmli. 1988. The metaphase scaffold is helically folded: sister chromatids have predominantly opposite helical handedness. *Cell.* 55:937–944.
7. Rattner, J. B., and C. C. Lin. 1985. Radial loops and helical coils coexist in metaphase chromosomes. *Cell.* 42:291–296.
8. Belmont, A. S., and K. Bruce. 1994. Visualization of G1 chromosomes: a folded, twisted, supercoiled chromonema model of interphase chromatid structure. *J. Cell Biol.* 127:287–302.
9. Belmont, A. S., J. W. Sedat, and D. A. Agard. 1987. A three-dimensional approach to mitotic chromosome structure: evidence for a complex hierarchical organization. *J. Cell Biol.* 105:77–92.
10. Kireeva, N., M. Lakonishok, I. Kireev, T. Hirano, and A. S. Belmont. 2004. Visualization of early chromosome condensation: a hierarchical folding, axial glue model of chromosome structure. *J. Cell Biol.* 166:775–785.
11. Sedat, J., and L. Manuelidis. 1978. A direct approach to the structure of eukaryotic chromosomes. *Cold Spring Harb. Symp. Quant. Biol.* 42:331–350.
12. Bernardi, G. 2000. Isochores and the evolutionary genomics of vertebrates. *Gene.* 241:3–17.
13. Furey, T. S., and D. Haussler. 2003. Integration of the cytogenetic map with the draft human genome sequence. *Hum. Mol. Genet.* 12:1037–1044.
14. Alberts, B. 2002. Molecular Biology of the Cell, 4th ed. Garland Science, New York.
15. Maeshima, K., and U. K. Laemmli. 2003. A two-step scaffolding model for mitotic chromosome assembly. *Dev. Cell.* 4:467–480.
16. Baumgartner, M., B. Dutrillaux, N. Lemieux, A. Lilienbaum, D. Paulin, et al. 1991. Genes occupy a fixed and symmetrical position on sister chromatids. *Cell.* 64:761–766.
17. Dietzel, S., and A. S. Belmont. 2001. Reproducible but dynamic positioning of DNA in chromosomes during mitosis. *Nat. Cell Biol.* 3:767–770.
18. Strukov, Y. G., Y. Wang, and A. S. Belmont. 2003. Engineered chromosome regions with altered sequence composition demonstrate hierarchical large-scale folding within metaphase chromosomes. *J. Cell Biol.* 162:23–35.
19. Robinett, C. C., A. Straight, G. Li, C. Willhelm, G. Sudlow, et al. 1996. In vivo localization of DNA sequences and visualization of large-scale chromatin organization using *lac* operator/repressor recognition. *J. Cell Biol.* 135:1685–1700.
20. Urlaub, G., P. J. Mitchell, E. Kas, L. A. Chasin, V. L. Funanage, et al. 1986. Effect of γ rays at the dihydrofolate reductase locus: deletions and inversions. *Somat. Cell Mol. Genet.* 12:555–566.
21. Tumbar, T., and A. S. Belmont. 2001. Interphase movements of a DNA chromosome region modulated by VP16 transcriptional activator. *Nat. Cell Biol.* 3:134–139.
22. Bickmore, W. A., and K. Oghene. 1996. Visualizing the spatial relationships between defined DNA sequences and the axial region of extracted metaphase chromosomes. *Cell.* 84:95–104.
23. Li, G., G. Sudlow, and A. S. Belmont. 1998. Interphase cell cycle dynamics of a late-replicating, heterochromatic homogeneously staining region: precise choreography of condensation/decondensation and nuclear positioning. *J. Cell Biol.* 140:975–989.
24. Valkov, N. I., J. L. Gump, and D. M. Sullivan. 1997. Quantitative immunofluorescence and immunoelectron microscopy of the topoisomerase II α associated with nuclear matrices from wild-type and drug-resistant Chinese hamster ovary cell lines. *J. Cell. Biochem.* 67:112–130.
25. Hiraoka, Y., J. R. Swedlow, M. R. Paddy, D. A. Agard, and J. W. Sedat. 1991. Three-dimensional multiple-wavelength fluorescence microscopy for the structural analysis of biological phenomena. *Semin. Cell Biol.* 2:153–165.
26. Pixton, J. L., and A. S. Belmont. 1996. NewVision: a program for interactive navigation and analysis of multiple 3D data sets using coordinated virtual cameras. *J. Struct. Biol.* 116:77–85.
27. Belmont, A. S. 2006. Mitotic chromosome structure and condensation. *Curr. Opin. Cell Biol.* 18:632–638.
28. Earnshaw, W. C., and M. M. Heck. 1985. Localization of topoisomerase II in mitotic chromosomes. *J. Cell Biol.* 100:1716–1725.
29. Gasser, S. M., T. Laroche, J. Falquet, E. Boy de la Tour, and U. K. Laemmli. 1986. Metaphase chromosome structure. Involvement of topoisomerase II. J. Mol. Biol. 188:613–629.
30. Cheezum, M. K., W. F. Walker, and W. H. Guilford. 2001. Quantitative comparison of algorithms for tracking single fluorescent particles. *Biophys. J.* 81:2378–2388.
31. Thompson, R. E., D. R. Larson, and W. W. Webb. 2002. Precise nanometer localization analysis for individual fluorescent probes. *Biophys. J.* 82:2775–2783.
32. Hirano, T. 2002. The ABCs of SMC proteins: two-armed ATPases for chromosome condensation, cohesion, and repair. *Genes Dev.* 16:399–414.
33. Giménez-Abián, J. F., I. Sumara, T. Hirota, S. Hauf, D. Gerlich, et al. 2004. Regulation of sister chromatid cohesion between chromosome arms. *Curr. Biol.* 14:1187–1193.
34. Sumner, A. T. 1991. Scanning electron microscopy of mammalian chromosomes from prophase to telophase. *Chromosoma.* 100:410–418.